Determination of Three-Dimensional Voxel Sensitivity for Two- and Three-Headed Coincidence Imaging

Edward J. Soares, Kevin W. Germino, Stephen J. Glick, *Member, IEEE*, and Robert Z. Stodilka, *Member, IEEE*

***Abstract*—Recently, SPECT and positron emission tomography imaging modalities have been hybridized so that positron coincidence detection can be accomplished with SPECT systems. Originally, only systems with two opposing camera heads were employed. Recent developments to improve sensitivity include the addition of a third camera head. Several authors have developed methods to calculate line-of-response and voxel sensitivities, known as rotational and geometric weights, respectively. These weights are important for use as normalization factors in iterative image reconstruction, as well as to provide insight into the nonuniformity of voxel sensitivity across the reconstructed field-of-view. Although their formulations use analytic expressions, the equations derived for the voxel sensitivities involve an integral which cannot be computed in closed form; that is, one must use a numerical approximation. This may affect the voxel sensitivity in that the accuracy and speed of such a discrete calculation are heavily dependent on the mesh size used. The authors' alternative approach, that does not rely on the numerical approximation, is to directly calculate the solid angle subtended by each voxel with the detectors over all detector positions. They include results for two camera heads 180° apart (DUAL), three camera heads 120° apart (TRI), and three camera heads 90° and 180° apart (C-SHAPE), with and without axial collimation.**

***Index Terms*—Geometric sensitivity, hybrid PET, positron coincidence detection, solid angle.**

I. Introduction

OVER the past several years, SPECT and positron emission tomography (PET) imaging technologies have been combined, resulting in the ability of SPECT systems to detect positron coincidence events. The first hybrid imaging systems utilized two opposing detectors. However, the need to improve sensitivity motivated the addition of a third detector head.

Researchers have previously developed methods to calculate line-of-response (LOR) and voxel sensitivities, known as rotational and geometric weights, respectively. The LOR sensitivity is a measure of how much each LOR contributes to the reconstructed volume, while the voxel sensitivity is a measure of how much each voxel contributes to the data. These sensitivity weights can be used as normalization factors in iterative image reconstruction or to give information regarding any nonuniformity in voxel sensitivity across the reconstructed field-of-view (FOV).

Reader *et al.* [1] derived an analytic expression for the sensitivity of each LOR (rotational weight) as a function of radial distance r from the center of the object in the trans-axial (x, y) slice, as well as the sensitivity of each voxel (geometric weight) as a function of both radial distance r and the distance z in the axial direction. These factors were computed for a three-dimensional (3-D) system geometry using two camera heads 180° apart. Swan [2] extended this work to consider those cases where the detectable angular range of oblique LORs is affected by the finite extent of the detectors perpendicular to the axis of rotation. D'Asseler *et al.* developed methods to compute both rotational and geometric weights for two-dimensional (2-D) [3] and 3-D [4] system geometries using two camera heads at arbitrary orientations and showing results for two camera heads 180° apart, three camera heads 120° apart, and three camera heads 90° and 180° apart. Subsequently, Stodilka and Glick [5] discretely calculated LOR sensitivities for multihead systems, for various numbers of gantry positions and restrictions on LOR acceptance angles. Although some of these formulations [1], [3], [4] use analytic methods, the expressions for the voxel sensitivities involve an integral which cannot be computed in closed form, and thus a numerical approximation is required. This will affect the computation of the voxel sensitivity, as the accuracy and speed of the numerical method will be heavily dependent on the mesh size used. If the mesh size is too coarse, the weight may not accurately represent the proper weighting for the total number of LORs that pass through the voxel and contribute to the data, while a finer mesh size may increase accuracy, as well as computation time.

Our theoretical approach that uses no numerical approximations directly calculates the total solid angle subtended by each voxel with the detector geometry over all detector positions. The sensitivity of a voxel is related to the number of LORs that pass through the voxel and intersect a detector pair over all gantry positions. Theoretically, an infinite number of LORs satisfy this condition. However, one measure that can be used is the solid angle subtended by the voxel with the detectors.

Manuscript received January 10, 2002; revised January 3, 2003. This work was supported by the National Cancer Institute under Grant 78573.

E. J. Soares is with the Department of Mathematics and Computer Science, College of the Holy Cross, Worcester, MA 01610 USA (e-mail: esoares@holycross.edu).

K. W. Germino was with the Department of Mathematics and Computer Science, College of the Holy Cross, Worcester, MA 01610 USA. He is now with the Medical Sciences Training Program, Northwestern University, Chicago, IL 60611 USA (e-mail: kgermino005@md.northwestern.edu).

S. J. Glick is with the Department of Radiology, Division of Nuclear Medicine, University of Massachusetts Medical School, Worcester, MA 01655 USA (e-mail: Stephen.Glick@umassmed.edu).

R. Z. Stodilka is with CareImaging Corporation, Mississauga, ON, Canada (e-mail: RStodilka@CareImaging.com).

Digital Object Identifier 10.1109/TNS.2003.812435

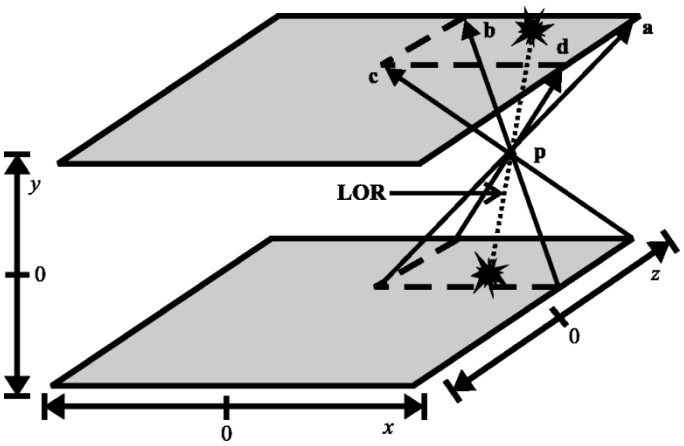

Fig. 1. The FOV defined by a voxel (a point $\mathbf{p} \in \mathbf{R}^3$) with two opposing detectors is characterized by four vectors, which we call $\mathbf{a}$, $\mathbf{b}$, $\mathbf{c}$, and $\mathbf{d}$.

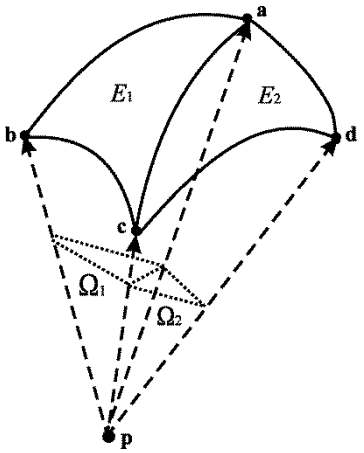

Fig. 2. Geometry illustrating the solid angle subtended by a point $\mathbf{p}$ with the detectors, as defined by the unit vectors $\mathbf{a}$, $\mathbf{b}$, $\mathbf{c}$, and $\mathbf{d}$. The solid angle Ω_1 is calculated as the area E_1 of the spherical triangle on the unit sphere determined by $\mathbf{a}$, $\mathbf{b}$, and $\mathbf{c}$, while the solid angle Ω_2 is calculated as the area E_2 of the spherical triangle on the unit sphere determined by $\mathbf{a}$, $\mathbf{d}$, and $\mathbf{c}$.

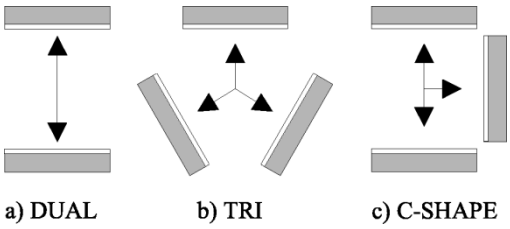

Fig. 3. Three hybrid PET camera configurations were studied: (a) two opposing camera heads 180° apart (DUAL configuration), (b) three camera heads 120° apart (TRI configuration), and three camera heads where the second head is offset from the first by 90°, and (c) the third head is offset from the first by 180° (C-SHAPE configuration).

II. Theory

The FOV defined by a voxel (a point $\mathbf{p} = (x_p, y_p, z_p) \in \mathbf{R}^3$) with the detectors for a particular gantry position is characterized by four vectors, which we call $\mathbf{a}$, $\mathbf{b}$, $\mathbf{c}$, and $\mathbf{d}$. The geometry for a typical FOV for a voxel is seen in Fig. 1.

Without loss of generality, we assume the origin of these four vectors is the center of the voxel under consideration and that each vector has unit length. If these conditions are not met, then one must subtract the voxel of interest $\mathbf{p}$ from the particular vector under consideration and then normalize the result. Any LOR within this FOV will pass through the voxel and intersect a detector pair, and thus the voxel will contribute to the data. Regardless of the size of the FOV, an infinite number of LORs will pass through the voxel and so counting the number of LORs is impossible. Thus, we consider a geometric measure of the FOV, namely the solid angle subtended by the voxel with the detectors (Fig. 2).

The total solid angle subtended by the voxel is defined by the sum of two solid angles Ω_1 and Ω_2. The solid angle Ω_1 is calculated as the area E_1 of the spherical triangle on the unit sphere determined by $\mathbf{a}$, $\mathbf{b}$, and $\mathbf{c}$, while the solid angle Ω_2 is calculated as the area E_2 of the spherical triangle on the unit sphere determined by $\mathbf{a}$, $\mathbf{d}$, and $\mathbf{c}$. From [6], the respective solid angles are found using

$$\tan\left(\frac{E_1}{2}\right) = \frac{|\mathbf{a}\cdot(\mathbf{b}\times\mathbf{c})|}{1+\mathbf{b}\cdot\mathbf{c}+\mathbf{c}\cdot\mathbf{a}+\mathbf{a}\cdot\mathbf{b}} \tag{1}$$

and

$$\tan\left(\frac{E_2}{2}\right) = \frac{|\mathbf{a}\cdot(\mathbf{d}\times\mathbf{c})|}{1+\mathbf{d}\cdot\mathbf{c}+\mathbf{c}\cdot\mathbf{a}+\mathbf{a}\cdot\mathbf{d}} \tag{2}$$

where $|\ |$ is the absolute value function, and $\cdot$ and $\times$ represent the dot product and cross product operations between vectors, respectively. Thus, for each point $\mathbf{p}$, we need to find four vectors, which subtend the maximum FOV with the detectors.

III. Methods

Three different hybrid-PET detector configurations were studied. The first was the arrangement of two opposing camera heads 180° apart (DUAL), the second was three camera heads 120° apart in an equilateral triangle arrangement (TRI), and the third was three camera heads where the second head is offset from the first by 90° and the third head is offset from the first by 180° in a C-shaped configuration (C-SHAPE). These arrangements can be seen in Fig. 3.

The overall goal is to compute the voxel sensitivity function $S(x, y, z)$ for each point in $\mathbf{R}^3$, for each detector configuration. Examining the cylindrical coordinate representation of a point (x, y, z)

$$\begin{aligned} x &= r\cos(\theta) \\ y &= r\sin(\theta) \\ z &= z \end{aligned} \tag{3}$$

we note that the voxel sensitivity is rotationally symmetric, and thus independent of polar angle θ within a trans-axial (x, y) slice. Thus, we may compress the spatial variables $\mathbf{x}$ and $\mathbf{y}$ into a radial variable r and compute the voxel sensitivity $S(r, z)$ for $0 \le z \le z_{\max}$ and $0 \le r \le r_{\max}$, where $z_{\max}$ is the maximum extent of the detectors in the axial direction and $r_{\max}$ is the radius of rotation of the detectors.

The general approach we take to determining the maximal FOV (and thus solid angle) for a given point and detector arrangement is via "region growing." By beginning with a minimally subtended solid angle and increasing the FOV size in-

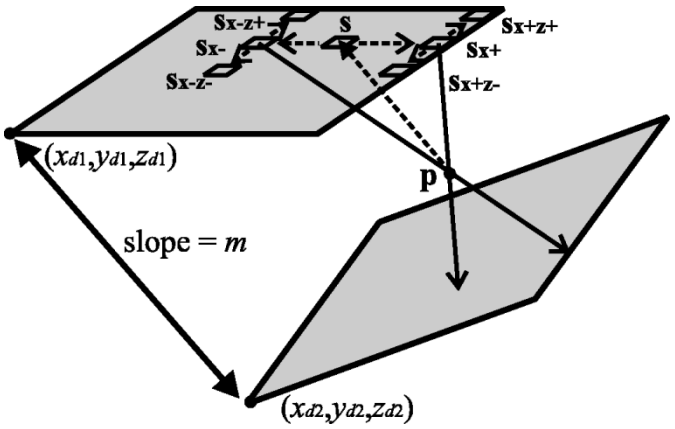

Fig. 4. Defining a seed vector $\mathbf{s}$ in order to determine the four vectors that subtend the point $\mathbf{p}$ with the detectors. The seed vector is then moved and bifurcated in the x and z directions to "grow" the maximal FOV.

crementally, we grow the subtended solid angle to its maximal capacity.

To compute the solid angle for a point $\mathbf{p}$, determined by particular r and z within the FOV of an arbitrary detector pair at gantry angle $\phi = 0$, we project $\mathbf{p}$ onto one of the camera heads (see Fig. 4) to define a seed point $\mathbf{s} = (x_s, y_s, z_s)$. To facilitate this, we rotate the entire geometry so that the detector onto which one is projecting is oriented on top.

We determine the seed point by computing the slope m of the line connecting corresponding detector edges

$$m = \frac{y_{d1} - y_{d2}}{x_{d1} - x_{d2}} \tag{4}$$

defining the equation of the line with slope m passing through the point $\mathbf{p}$, and then extrapolating to the top head via

$$\begin{aligned} x_s &= \frac{y_s - y_p}{m} + x_p \\ y_s &= r_{\max} \\ z_s &= z_p. \end{aligned} \tag{5}$$

Next, we bifurcate $\mathbf{s}$ in the positive and negative x directions resulting in

$$\begin{aligned} \mathbf{s}_{x+} &= \mathbf{s} + (p\text{size}, 0, 0) \\ \mathbf{s}_{x-} &= \mathbf{s} - (p\text{size}, 0, 0). \end{aligned} \tag{6}$$

Beginning with $\mathbf{s}_{x+}$ and $\mathbf{p}$, we extrapolate along the line joining these points, until we find the point that lies in the plane of the opposing detector. The process of extrapolation along a line defined by two points is found in [7]. If the extrapolated point lies within the bounds of the opposing detector, then $\mathbf{s}_{x+}$ is kept and then is moved incrementally in the positive $\mathbf{x}$-direction toward the edge of the detector

$$\mathbf{s}_{x+} = \mathbf{s}_{x+} + (p\text{size}, 0, 0). \tag{7}$$

This procedure is done until the extrapolated point determined by $\mathbf{s}_{x+}$ and $\mathbf{p}$ no longer lies within the bounds of the opposing detector, or if $\mathbf{s}_{x+}$ has been moved past the edge of the detector. The same procedure is also conducted for $\mathbf{s}_{x-}$ using

$$\mathbf{s}_{x-} = \mathbf{s}_{x-} - (p\text{size}, 0, 0). \tag{8}$$

Once the movements of these two points in their respective x directions have been exhausted, the updated points $\mathbf{s}_{x+}$ and $\mathbf{s}_{x-}$ are then each bifurcated in the positive and negative z-directions, creating four points

$$\begin{aligned} \mathbf{s}_{x+z+} &= \mathbf{s}_{x+} + (0, 0, p\text{size}) \\ \mathbf{s}_{x+z-} &= \mathbf{s}_{x+} - (0, 0, p\text{size}) \\ \mathbf{s}_{x-z+} &= \mathbf{s}_{x-} + (0, 0, p\text{size}) \\ \mathbf{s}_{x-z-} &= \mathbf{s}_{x-} - (0, 0, p\text{size}). \end{aligned} \tag{9}$$

Analogously, each of these points is then tested using $\mathbf{p}$ and the extrapolation procedure, and moved incrementally in its respective z direction. Once the four points that subtend the maximal FOV are found, we assign

$$\begin{aligned} \mathbf{a} &= \frac{\mathbf{s}_{x+z+} - \mathbf{p}}{||\mathbf{s}_{x+z+} - \mathbf{p}||} \quad \mathbf{b} = \frac{\mathbf{s}_{x-z+} - \mathbf{p}}{||\mathbf{s}_{x-z+} - \mathbf{p}||} \\ \mathbf{c} &= \frac{\mathbf{s}_{x-z-} - \mathbf{p}}{||\mathbf{s}_{x-z-} - \mathbf{p}||} \quad \mathbf{d} = \frac{\mathbf{s}_{x+z-} - \mathbf{p}}{||\mathbf{s}_{x+z-} - \mathbf{p}||}. \end{aligned} \tag{10}$$

The solid angles E_1 and E_2 are then computed using (1) and (2).

This process is continued for all orientations (gantry positions) of the detectors and the sum total of all solid angular contributions have been accounted for. If the system geometry is comprised of more than two camera heads, then this process must be done for all camera pairs individually, and then the results combined to form the total solid angle for each voxel. The reader may note that the computation and testing of the vectors can be accomplished more easily by clock-wise rotation of the point $\mathbf{p}$, rather than counter clock-wise rotation of the detectors, when considering gantry positions other than $\phi = 0$.

One of the major problems with hybrid PET is a limited count-rate capability, which ultimately limits the number of coincidences that are measured. Count-rate limitations are especially problematic for large FOV, rotating gamma cameras with NaI scintillators, because only a small fraction of photons detected are typically paired with their corresponding coincidence photon. In other words, a very large number of single photons are incident on the detectors. One approach for reducing this large number of singles incident on the detector is to use axial collimation or septa. This idea is similar to that used in conventional PET cameras operating in 2-D mode. By placing axial collimators on each detector head, the maximum axial angle of incidence $\alpha_{\max}$ for an LOR can be expressed as

$$\alpha_{\max} = \tan^{-1}\left(\frac{SS}{SL}\right) \tag{11}$$

where SS is the septal spacing and SL is the septa length. In this study, the effect of axial collimation on voxel sensitivity is investigated by assuming that all LORs must have axial incidence angles that are less than the maximum angle constraint imposed by the septa. Septal penetration is not modeled.

In our experiments, we chose our system parameters to model the Marconi IRIX camera, namely a width (x) of 53.5 cm, length (z) of 37.1 cm, and radius of rotation (y) of 34.0 cm. We employed 120 gantry positions over 180° for the DUAL configuration and 120 gantry positions over 360° for the TRI and C-SHAPE configurations. The voxel sensitivity was

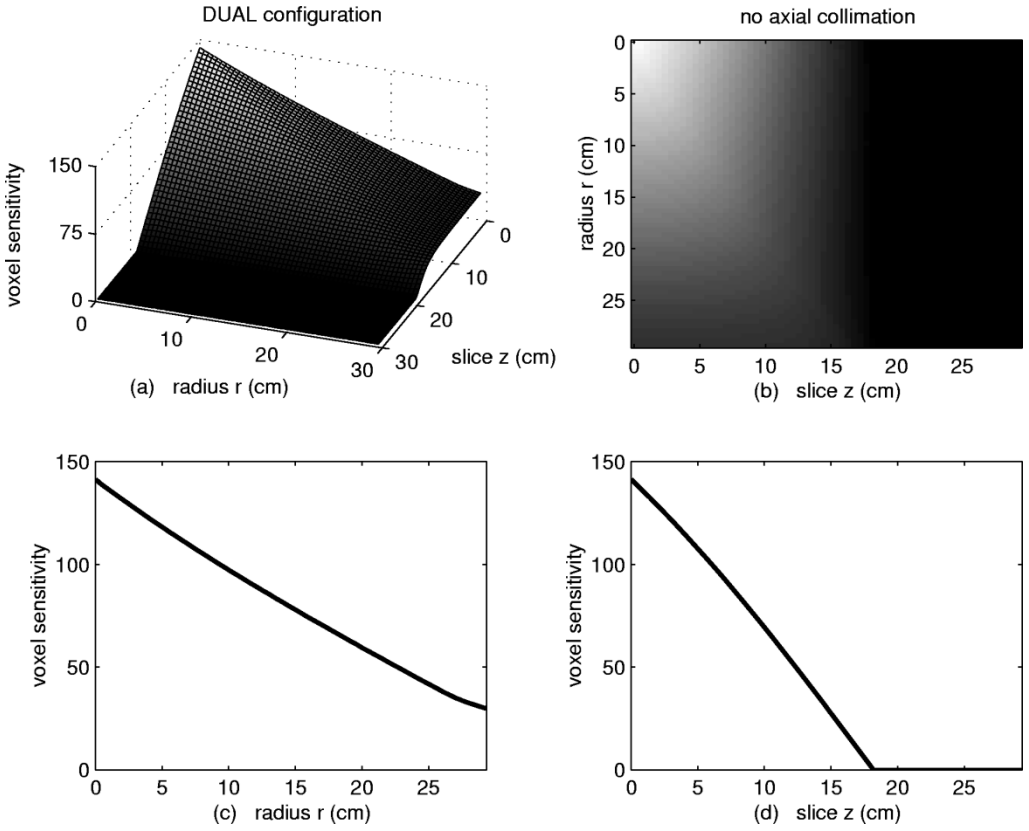

Fig. 5. Voxel sensitivity as a function of radius r from the center of rotation and axial slice z for two camera heads 180° apart (DUAL) with no axial collimation.

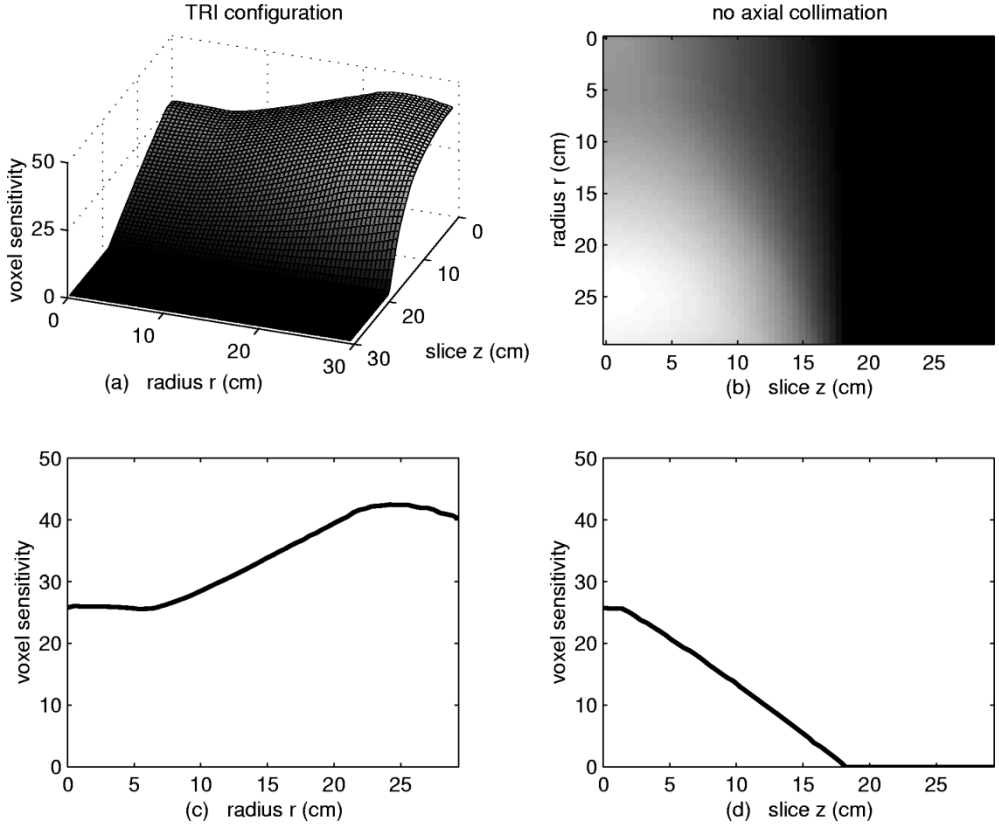

Fig. 6. Voxel sensitivity as a function of radius r from the center of rotation and axial slice z for three camera heads 120° apart (TRI) with no axial collimation.

computed for a 64×64 array with pixel size 0.466 cm/pixel ($128 \times 128 \times 128$ reconstructed volume). When modeling axial collimation, we studied a septal length of 3.5 cm, septal width of 0.23 cm, and a septal spacing of 1.0 cm, on center.

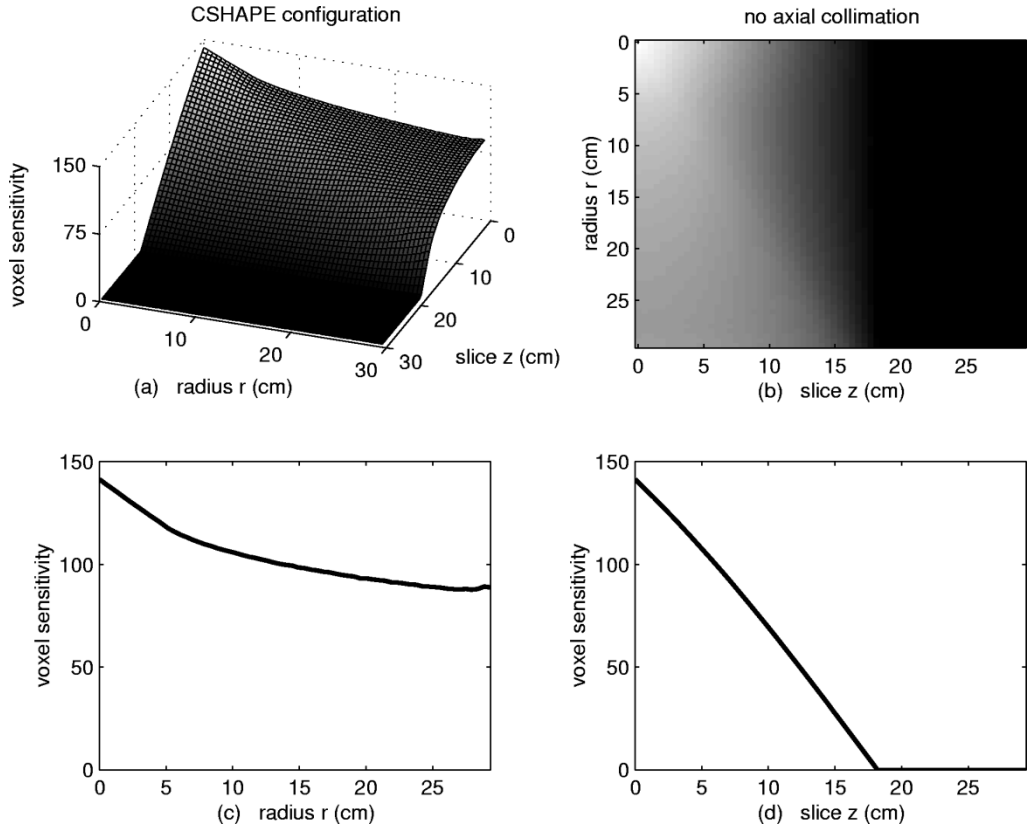

Fig. 7. Voxel sensitivity as a function of radius r from the center of rotation and axial slice z for three camera heads 9° and 180° apart (C-SHAPE) with no axial collimation.

IV. Results

The results of determining voxel sensitivity for the DUAL, TRI, and C-SHAPE configurations, with and without axial collimation, are shown in Figs. 5–10. Figs. 5–7 comprise voxel sensitivity results when no axial collimation is used, while Figs. 8–10 display results when axial collimation is used, where the septa are spaced 1.0 cm apart, on center. For each voxel sensitivity function $S(r,z)$, we display our results as (a) surface plots, (b) gray scale images, (c) radial profiles $(z=0)$, and (d) axial profiles $(r=0)$, for each of the three detector configurations, respectively.

In the DUAL configuration (Fig. 5), as radial distance r from the origin increases, voxel sensitivity decreases approximately linearly. This decrease in voxel sensitivity is also seen when axial position z increases away from the origin. This is due to the effect of the finite extent of the detectors in both x and z on decreasing the solid angle subtended by the voxel with the detectors.

In the TRI configuration (Fig. 6), voxel sensitivity is fairly flat close to the origin, begins to increase with radial distance r, peaks, and then decreases as we move beyond the extent of the detectors. This is because points in the middle of the object will subtend a smaller solid angle, as the camera heads are not directly opposing each other. As in the DUAL case, voxel sensitivity decreases when axial position z increases away from the origin.

When the cameras are arranged in the C-SHAPE configuration (Fig. 7), voxel sensitivity is slightly peaked in the center, falls off approximately linearly as radial distance r increases, and then flattens out as we move toward the extent of the detectors. This is due to the fact that the C-SHAPE configuration is the sum of contributions from a DUAL configuration and from two other different pairs of detectors, where each pair is offset by 90° [see Fig. 3(c)]. From the DUAL case results, voxel sensitivity falls off linearly as radial distance increases. When just considering either of the two detectors offset by 90°, the solid angle contribution increases linearly with radial distance, although at a much lower magnitude than the DUAL contribution. Thus the sum of the contributions from the two different detector pairs offset by 90° increases the solid angle contribution at the periphery, resulting in a flatter graph at the edge. As in the previous cases, voxel sensitivity decreases approximately linearly when axial position z increases away from the origin.

We then considered the effect of axial collimation on the voxel sensitivity. Axial septa restrict incident LORs in the z-direction and thus should reduce the maximal solid angle that a voxel can subtend. This effect was studied for axial septa spaced 1.0 cm apart, on center. The results are displayed for the three different detector configurations in Figs. 8–10.

From these results, it can be seen that axial collimation has the effect of flattening the voxel sensitivity in the axial direction for z values away from the edge of the detector, for each of the three detector configurations. This is due to the fact that the septa restrict the extent of acceptable LORs in the axial direction. Thus, for voxels closer to the center of the object, the extent of the detectors in the z direction plays no role in restricting the acceptable LORs. It is only when the voxel is closer

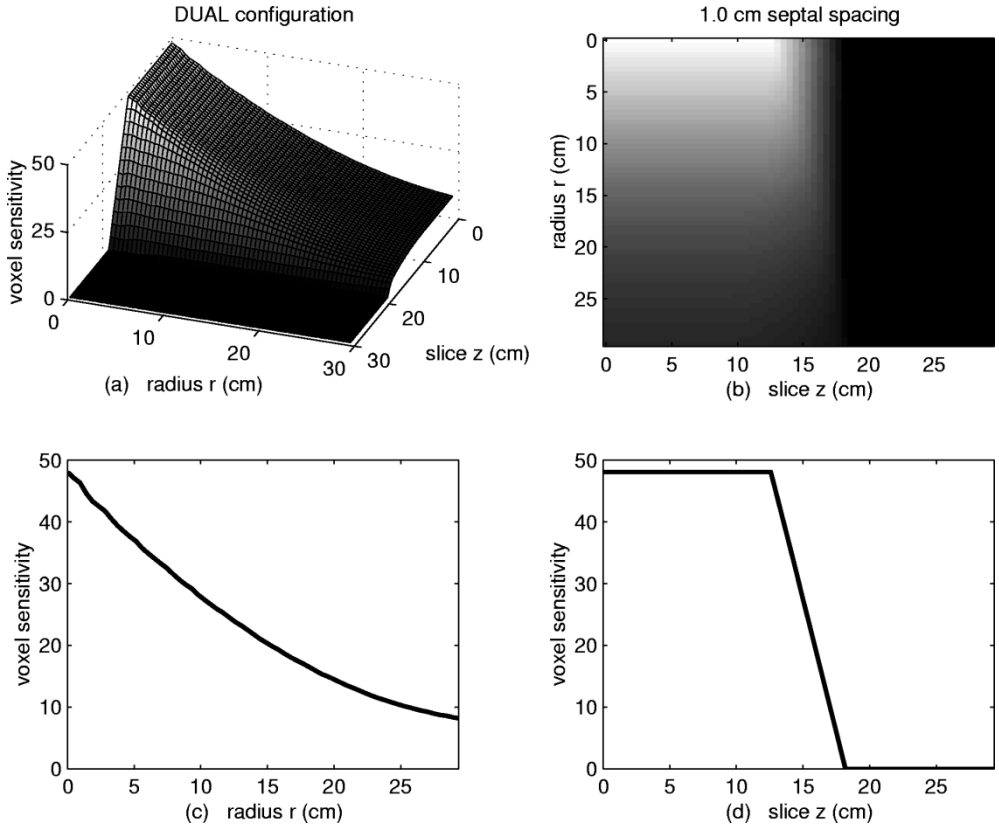

Fig. 8. Voxel sensitivity as a function of radius r from the center of rotation and axial slice z for two camera heads 180° apart (DUAL) with axial collimation. The septa are spaced 1.0 cm apart, on center.

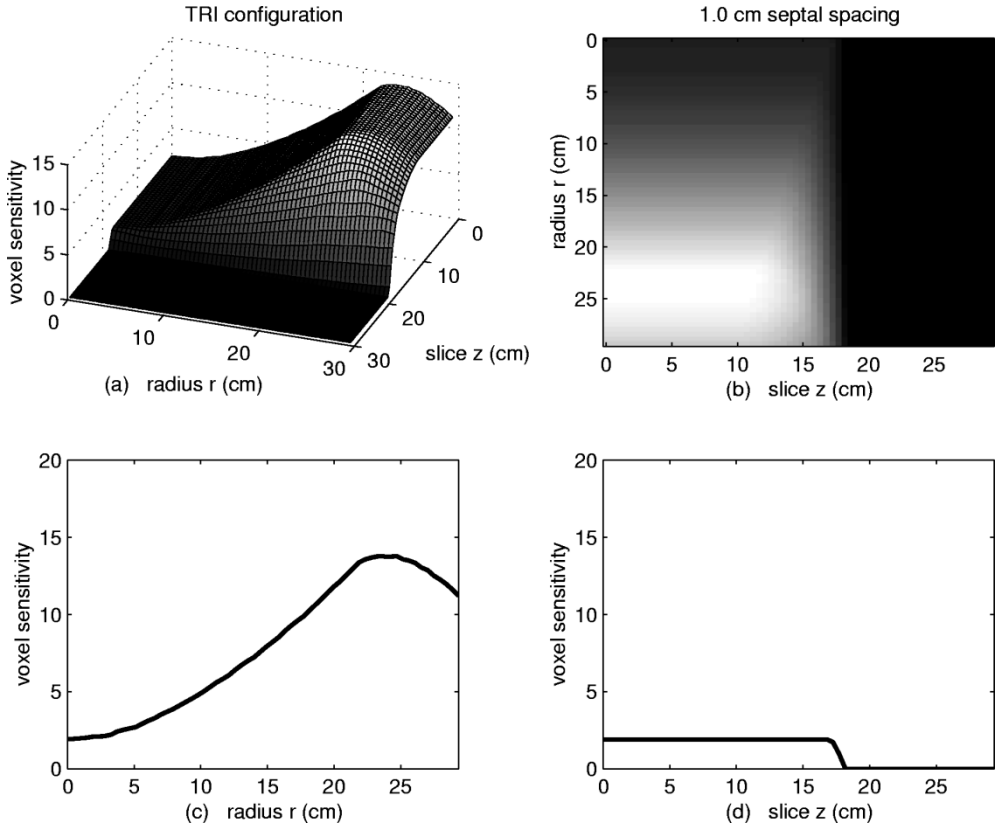

Fig. 9. Voxel sensitivity as a function of radius r from the center of rotation and axial slice z for three camera heads 120° apart (TRI) with axial collimation. The septa are spaced 1.0 cm apart, on center.

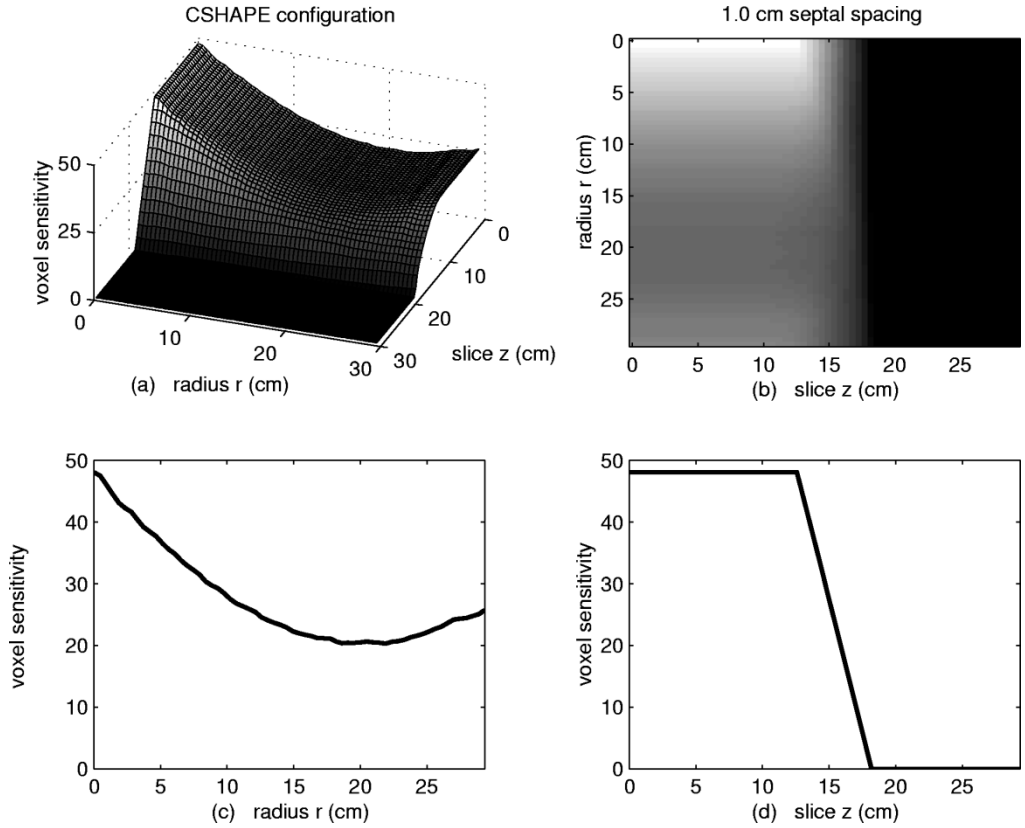

Fig. 10. Voxel sensitivity as a function of radius r from the center of rotation and axial slice z for three camera heads 90° and 180° apart (C-SHAPE) with axial collimation. The septa are spaced 1.0 cm apart, on center.

to the edge of the object in the axial direction that the detector extent influences the acceptability of the LORs. It should also be noted that the basic shape of the voxel sensitivity function remains unchanged in the radial direction, for all three detector configurations. This is expected, as the axial collimation places no restrictions on LORs within the trans-axial slice.

V. Discussion

Two important points to observe are which detector configuration provides the least nonuniform sensitivity across the reconstructed FOV and which yields the highest level of sensitivity. In the case of no collimation, we note that all three methods are highly nonuniform axially. However, voxel sensitivity for the C-SHAPE configuration does vary less radially, when compared with the DUAL and TRI configurations. In addition, both the DUAL and C-SHAPE configurations possess about three times the sensitivity of the TRI configuration, at maximum value. When axial collimation is incorporated into the analysis, we see that its effect is to reduce the nonuniformity of the voxel sensitivity function axially, for all three configurations. It also has the effect of reducing the level of sensitivity radially for the DUAL and C-SHAPE configurations by a factor of three. The sensitivity for the TRI configuration is reduced by a factor of ten close to the origin and by a factor of three at the periphery.

One effect that was not addressed in our analysis is septal penetration. In theory, axial collimation will restrict the detection of photons with an angle of incidence greater than $\alpha_{\max}$. However, in practice, a significant number of the 511 KeV photons do penetrate the septa and thus will contribute to the data. Thus, to accurately determine voxel sensitivity across the FOV of the detectors, it is important to account for the effect of septal penetration. Unfortunately, a method to accurately incorporate this phenomenon into our analytic formulation eludes us. Toward this end, we continue to investigate septal penetration using Monte Carlo methods.

VI. Conclusion

We have developed an analytic method to compute 2-D voxel sensitivity factors for two- and three-headed coincidence imaging. The method involves computing the total solid angle subtended by each point in the object with the detectors. The advantage to this methodology is that no numerical integration techniques are needed to estimate the contribution each voxel makes to the data. This methodology can be extended to any number of detector pairs in a variety of configurations.

Acknowledgment

The authors would like to thank Y. D'Asseler and S. Vandenberghe of the Department of Electronics and Information Systems, Ghent University, and J. Little, Ph.D., and D. Conti of the Department of Mathematics and Computer Science, College of the Holy Cross, for their useful comments and suggestions.

REFERENCES

[1] A. Reader, K. Erlandsson, M. A. Flower, and R. J. Ott, "Fast accurate iterative reconstruction for low-statistics positron volume imaging," *Phys. Med. Biol.*, vol. 43, pp. 835–846, 1998.

[2] W. L. Swan, "Exact rotational weights for coincidence imaging with a continuously rotating dual-headed gamma camera," *IEEE Trans. Nucl. Sci.*, vol. 47, pp. 1660–1664, Aug. 2000.

[3] Y. D'Asseler, S. Vandenburghe, M. Koole, L. Bouwens, R. Van de Walle, I. Lemahieu, and R. A. Dierckx, "Geometric sensitivity calculation of three-headed gamma camera-based coincidence detection," in *SPIE Medical Imaging 2000, Physics Medical Imaging*, vol. 3977, Proc. SPIE, pp. 58–67.

[4] Y. D'Asseler, S. Vandenburghe, C. G. Matthews, R. Van de Walle, I. Lemahieu, and R. A. Dierckx, "Three-dimensional geometric sensitivity calculation for three-headed coincidence imaging," *IEEE Trans. Nucl. Sci.*, vol. 48, pp. 1446–1451, Aug. 2001.

[5] R. Stodilka and S. Glick, "Evaluation of geometric sensitivity for hybrid PET," *J. Nucl. Med.*, vol. 42, no. 7, pp. 1116–1120, 2001.

[6] F. Eriksson, "On the measure of solid angles," *Math. Mag.*, vol. 63, no. 3, pp. 184–187, June 1990.

[7] R. Siddon, "Fast calculation of the exact radiological path for a three-dimensional CT array," *Med. Phys.*, vol. 12, no. 2, pp. 252–255, Mar./Apr. 1985.